Published in "Physical Review B: 71, 153403, 2005"
which should be cited to refer to this work.

Charge-density oscillation on graphite induced by the interference of electron waves

P. Ruffieux,[1,2,*] M. Melle-Franco,[3] O. Gröning,[1] M. Bielmann,[1] F. Zerbetto,[3] and P. Gröning[1,2]
[1]*Swiss Federal Laboratories for Materials Testing and Research, Überlandstrasse 129, 8600 Dübendorf, Switzerland*
[2]*Physics Department, University of Fribourg, Pérolles, 1700 Fribourg, Switzerland*
[3]*Dipartimento di Chimica "G. Ciamician," Universitá degli Studi di Bologna, V. F. Selmi 2, 40126 Bologna, Italy and INSTM, Bologna, Italy*
(Received 13 September 2004; revised manuscript received 8 February 2005; published 22 April 2005)

We report on a pronounced redistribution of the local electronic density of states at the graphite surface, which is induced by the presence of low energy hydrogen-ion induced point defects. Scanning tunneling microscopy reveals standing waves in the local density of states, which are due to backscattering of electron wave functions at individual point defects. The superstructure thereby formed is directly related to the pointlike structure of the Fermi surface of graphite. For high defect density interference patterns are observed which sensitively change structure on the relative positions of the defects. These patterns could be reproduced by tight binding simulations of various defect distributions.

DOI: 10.1103/PhysRevB.71.153403 PACS number(s): 73.61.Wp, 61.72.Ji, 68.37.Ef

The presence of defects induce strong modifications on the local electronic properties of cristalline solids. These modifications have been thoroughly investigated on metal surfaces where they are known as Friedel oscillations and manifest as standing waves on the electronic density spanning regions up to ~10 nm from the defects.[1–3] The observed standing wave patterns on metals and high temperature superconductors could be linked to the electronic structure even for complex patterns.[4–6] The long range character of the electronic density standing waves allows, for instance, for indirect interaction between atoms adsorbed on surfaces, leading to adsorbate overlayer structures showing the same periodicity as the oscillations.[2] Similar long range oscillations have also been observed on graphite surfaces[7–9] and in carbon nanostructures[10–12] where they have even been used for the realization of single molecular electronic devices.[12] In this work we report on the scattering of graphite π-electrons due to single and multiple point defects as observed by STM. The high density of defects, due to the multiple scattering of the electrons, produces a rich variety of patterns strongly departing from the ones observed from isolated defects. Experimental findings will be compared with two models, one phenomenological, based on the superposition of plane waves and one explicit, based on tight binding (TB) simulations that will allow us to address different aspects of point defect scattering in graphite.

Samples of highly oriented pyrolithic graphite (HOPG, quality ZYB) were cleaved *in situ* under ultrahigh vacuum conditions. Exposure of the clean graphite surface to a H_2 electron cyclotron resonance (ECR) plasma created stochastically distributed point defects. A typical ion dose used for the treatment was of the order of 10^{13} ions/cm^{-2}. The average ion energy of ~2 eV, has been determined with an electrostatical analyzer. After plasma treatment, the sample was transferred to the vacuum-connected atomic force/scanning tunneling microscope (AFM/STM, Omicron) working under ultrahigh vacuum conditions at room temperature. Measurements were performed in the combined AFM/STM mode using the normal force as feedback signal and applying a fixed bias voltage between the sample and the tip. The recording of the piezo *z*-position and the tunneling current allows the simultaneous determination of the topography and the LDOS. For this measurement mode we used AFM tips coated with highly conductive boron doped CVD-diamond. In the absence of defects the usual trigonal structure with maxima in the LDOS on every second atom of the top layer is observed.[14]

Figure 1 shows an overview current image (U=70 mV) of a sample that has been exposed to H_2-plasma for 3 s. The

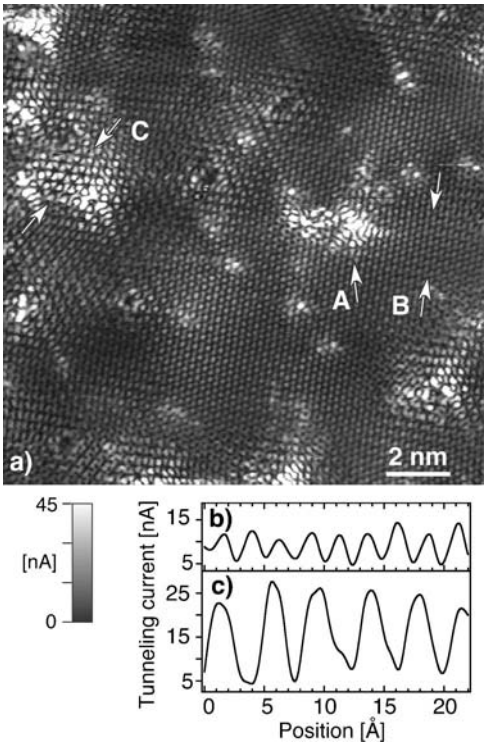

FIG. 1. (a) Current image of sample treated with H_2 plasma. The observed defect density is of the order of 20 per 100 nm^2. The data is recorded in the AFM constant force mode with a gap voltage of 70 mV. The scan range is 16×16 nm^2. The arrow A marks the position of a vacancy type defect. (b) Line cut at position B showing the undisturbed lattice. (c) Line cut at position C where the LDOS is dominated by the $\sqrt{3}$-superstructure.

hydrogen plasma treatment results mainly in the formation of two kind of defects, firstly chemisorbed hydrogen on the basal plane of graphite and secondly single atomic vacancies.[8,13] The number of observed carbon vacancies was four times lower than the number of hydrogen chemisorption sites. Both types of defects lead to a strong modification of the local electronic structure near the Fermi level, as observed in the current image. The symmetry of the short-ranged ($\sim$1 nm) modifications is related to the geometric structure of the defect.[7] In particular, atom vacancies have been shown to give rise to a local charge enhancement having a threefold symmetry, reflecting the nearest-neighbor directions of the defect site. Besides of these very local modifications, defects also mediate a redistribution of the electron density on a larger scale. For chemisorbed and vacancy type defects on graphite, the characteristic length of modifications of the electronic charge density was found to be $\sim$5 nm. The observed standing waves have a periodicity larger than, but commensurate with the underlying graphite lattice. From the Fast Fourier Transform (FFT) of current images in the vicinity of defects, the electron density reconstructs as a $(\sqrt{3} \times \sqrt{3})R30°$ superlattice. The extent of the charge redistribution near defects is seen in the enhanced corrugation of the current signal. Comparing line profiles of the undisturbed lattice [Fig. 1(b)] with line profiles of a region where the $\sqrt{3}$-superstructure dominates (c), an enhancement of the current corrugation by a factor of about 3 is found.

To understand the origin of the $(\sqrt{3} \times \sqrt{3})R30°$-superstructure induced by defects a closer look at the electronic structure of graphite is needed. The Fermi surface of graphite consists of small electron and hole pockets enclosing a very small volume. These pockets are centered at the corners of the Brillouin zone (BZ), i.e., at the **K** points. Figure 2(c) shows the calculated band structure of graphite for the high-symmetry line Γ-K. The Fermi energy (E_F) electrons have wave vectors $k_F = 4\pi/3a$ directed towards a corner of the Brillouin zone [where a is the lattice constant of graphite ($a = 2.46$ Å)]. At the **K** point, the interaction between the graphene layers, though weak, lifts the degeneracy of the π bands which results in a splitting of 0.7 eV for the π band related to the α-atom (located above an atom of the adjacent layer), whereas the π band related to the β-atom remains unchanged [Fig. 2(c)]. Along the **K**-**H** line, the β-related π band is localized on the β-atom with $E = E_F$, whereas the α-related π band is dispersive.[14] It has been proposed that the asymmetry between α and β sites observed in STM images of graphite results from the fact that the STM maps the local density of states integrated along the **K**-**H** line.[14] However, we like to point out that the imaging mechanism of STM on graphite is still controversially discussed and that also mechanical interactions between the surface atoms and the tip apex atoms need to be considered.[15]

For graphite, backscattering of electrons at surface steps or point defects is possible via two scattering channels. First, small momentum scattering, which is possible via coupling between bands crossing at the **K** point, since their opposite slopes describe a forward and a backward moving channel. Small momentum scattering locally conserves the lattice periodicity, although not necessarily the rotational symmetry,

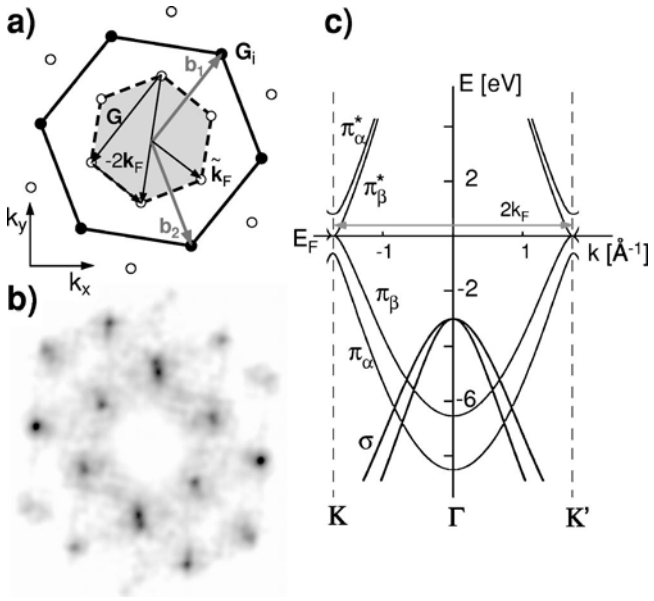

FIG. 2. (a) Two-dimensional reciprocal space with Brillouin zone (grey area) and reciprocal lattice vectors $\mathbf{b}_1$ and $\mathbf{b}_2$. The Fermi wave vectors are given by the corners of the Brillouin zone. (b) Two-dimensional Fourier transform of the current image shown in Fig. 1. The spots forming the inner hexagon represent the $\sqrt{3}$-superstructure observed in the vicinity of defects. Spots forming the larger hexagon rotated by 30° appear at wave vectors that correspond to reciprocal lattice vectors **G**. The outermost spots arise from the second harmonic of the inner hexagon. The spot at $\mathbf{k} = 0$ is due to the local charge enhancement at the defects sites and has been removed for better visibility of the relevant features. (c) Band structure of graphite along the high-symmetry line Γ-K (Ref. 16). π_α and π_β denote π bands related to the α- and β-atom, respectively. The momentum change required for large momentum scattering is indicated.

as found by simulations for carbon nanotubes.[17] The second possibility for reflection at defects is large momentum scattering between two opposite **K** points. In this case, the momentum changes from **K** to **K′** which corresponds to $\mathbf{q} = -2\mathbf{k}_F$. On metals large momentum scattering of surface states is responsible for the formation of Friedel oscillations. Since in these cases the surface state electrons behave like a quasi-free electron gas, there is no definite relation between $\mathbf{k}_F$ and the reciprocal lattice vectors and oscillations in these systems are not commensurate with the underlying atomic lattice.[3] In contrast, for graphite there is a definite relation between the lattice and the Fermi wave vectors, since they coincide with the corners of the BZ. The relation between the momentum change for large momentum scattering and the lattice parameter is given by $q = 2k_F = 8\pi/3a$. The required momentum change is reduced to $\mathbf{q} = \tilde{\mathbf{k}}_F$ if an appropriate reciprocal lattice vector is taken into account: $\mathbf{q} = -2\mathbf{k}_F = \tilde{\mathbf{k}}_F + \mathbf{G}$ [Fig. 2(a)]. Therefore, a modulation of the LDOS with a wavelength that corresponds to the Fermi wavelength $\lambda_F = 3a/2$ is expected for large momentum scattering on graphite.

Figure 2(b) shows the Fast Fourier transform (FFT) of the large scale current image, Fig. 1. Compared to a FFT of the

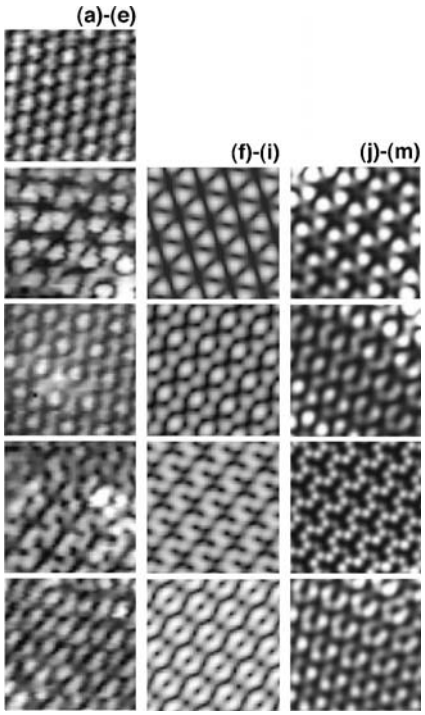

FIG. 3. (a)–(e) Experimental current images recorded with a gap voltage of 70 meV. The individual images display regions that are present in the overview image (Fig. 1). The scan range for each image is 17.5×17.5 Å^2. (f)–(i) Calculated spatial maps of $|\psi(\mathbf{r})|^2$ according to Eq. (1). Appropriate values of the complex numbers ϕ_j have been selected to match the experimentally observed pattern. (j)–(m) TB simulation of the LDOS in the vicinity of defects for various defect combinations (see text).

unperturbed lattice, new peaks appear at smaller wave vectors which match the corners of the Brillouin zone, i.e. the Fermi wave vectors. In the real space image, this superstructure is observed as a $(\sqrt{3}\times\sqrt{3})R30°$ modulation of the LDOS in the vicinity of defects. This shows the direct relation existing between the Fermi surface contour and the observed pattern of the standing waves in the vicinity of scatterers. The observed pronounced $\sqrt{3}$-superstructure in the LDOS indicates that large momentum scattering is the dominant reflection mechanism in the presence of point defects on graphite.

On samples with low defect density a decay of the intensity on the superstructure spots in the FFT is observed. In fact, for isolated defects, the superstructure extends over a typical range of 20–25 lattice constants and the phase, amplitude, and decay of the standing wave reflect the structure and symmetry of the defect, which could, in principle, be used for the identification of defects.[3,7] For increased defect densities new standing waves in the LDOS will be expected due to scattering from different defects. In our sample such patterns have been observed on defects typically 20 Å apart. Figure 3 shows small area details of the overview current image shown in Fig. 1(a). The images displayed in (b)–(e) are recorded in-between defects separated by only a few nm's. These areas are all dominated by the $\sqrt{3}$-superlattice contribution and show the variety of patterns in the LDOS originating from different defects relative positions. For comparison, the current image of a region with low defect density is given in (a) showing the usual graphite lattice periodicity described by the reciprocal lattice vectors $\mathbf{G}_i$.

The pointlike nature of the scattering defects results in the conservation of the phase relation only along the connecting line between two scattering centers. For all other directions the geometric phase shifts will vary with position resulting in spatially changing interference patterns.

The observed patterns could be reproduced by a model of superposed plane waves suggesting a local description of the states near the Fermi level of the form of

$$\psi(\mathbf{r}) = \sum_{j=1}^{6} \phi_j e^{i\mathbf{k}_{Fj}\cdot\mathbf{r}}, \qquad (1)$$

where ϕ_j are complex amplitudes representing the different contributions to the standing wave pattern. These amplitudes implicitly include the scattering phase shift at the defects and the geometrical phase shift, which depends on the relative position to the defects.[19]

The coefficients have been fitted in order to reproduce the experimentally observed LDOS where images (f)–(i) of Fig. 3 show the calculated spatial distribution of $|\psi(\mathbf{r})|^2$ using Eq. (1). The good agreement between the calculated and the measured LDOS confirms the validity of this model for the description of the standing wave due to multiple point defect scatterers in graphite. It also shows that the LDOS in the region between defects is dominated by standing waves with Fourier components that correspond to the Fermi wave vectors $\mathbf{k}_{Fj}$. Together with the absence of rotational symmetry breaking for isolated defects,[8,18] this evidences large momentum scattering as being the dominant channel for reflection at point defects.

The effect of the graphite defects was also simulated quantum chemically with a π-electron tight-binding model that implements periodic boundary conditions through Green functions.[7,20] The objective of these calculations was to evaluate directly the patterns that arise from the different relative positions, distances, and nature of the vacancy sites, (α or β).

In line with a previous report,[20] a single vacancy enhances the electron density near the Fermi level of the sites of opposite nature. In particular, some of the α sites, not visible at low bias in nondefective graphite, become visible in the presence of a nearby β vacancy, while α vacancies further enhance β carbon atoms, which are the only ones visible in the absence of defects.

The different patterns were obtained displacing systematically two defects in a graphite unit cell containing 2918 atoms and a linear dimension of 66 Å. Test simulations were also performed on a system comprising 6400 atoms yielding similar patterns.

As an example, the quantum chemical images of four double vacancy cases are illustrated in Figs. 3(j)–3(m). The defect positions are defined by two parameters, the distance, and, in analogy with the widely accepted structural description of carbon nanotubes, the angle θ,[21] which can vary between 0 and 30°. From Figs. 3(j)–3(m), the cases considered are β-β, α-β, β-β, α-β, with distances 29.52 Å, 29.34 Å, 33.27 Å, and 31.14 Å, and angles 0, 22.78°, 3.67°, and 9.19°.

The quantum chemical calculations on a cell with two vacancies yield four motifs that are remarkably different from one another despite the relatively small geometrical differences. They therefore show that slight variations of the relative positions of the defects induce strong changes in the patterns. Interestingly, three cases closely match the experiments.

Further physical insight emerges lowering the bias in the simulations below 0.05 eV. This is equivalent to consider contributions only from levels at/near the Fermi energy. At these low biases, single vacancy presents contributions to the LDOS only from sites of opposite nature and defects on both sites produce equivalent patterns. The same occurs for double vacancies where α-α and β-β have also equivalent images. In fact the only differences between patterns are (1) the absolute value of the electronic density (larger for α sites) and (2) the orientation of the standing wave pattern near the defect.[20] The equivalence of the calculated pattern shows that the scattering phase shift for α and β single vacancies and for same site vacancy pairs are the same at the Fermi energy. Notice that this differs for α-β pairs.

In conclusion, we have observed a marked redistribution of the LDOS in the vicinity of point defects on the graphite surface. The point defects, consisting of hydrogen chemisorbed sites and atomic vacancies, break the lattice symmetry and act as scatterers for the delocalized electrons. The resulting standing waves have wave vectors that correspond to the Fermi wave vectors $\mathbf{k}_{Fj}$ and are thus observed as a $\sqrt{3}$-superstructure in the tunneling current image. For isolated defects, the typical range observed for the charge redistribution is of $\sim$5 nm. For samples with high defect densities we observe a variety of patterns in the LDOS which depart from the single defect ones and depend on the relative position of the point defects. The experimentally observed patterns in the LDOS could be locally reproduced by a simulation where the standing waves are described as a superposition of plane waves having wave vectors that correspond to the corners of the first BZ, indicating large momentum scattering as the dominant channel for reflection at point defects.

TB simulations of different configurations of carbon vacancies also reproduced the experimental patterns revealing a strong dependence on these patterns, with subtle changes in the LDOS for small variations of the relative position of defects. At the Fermi energy single α and β vacancies have the same scattering phase shift. Analogously, α-α and β-β defect give equivalent patterns which shows that the phase shift may be conserved also in the case of multiple scattering.

Besides the influence on the transport properties due to scattering at the point defects, a modulation of the local reactivity for chemically adsorbing atoms has to be expected due to the marked redistribution of the LDOS in the vicinity of the defects.

We thank the Swiss National Science Foundation (MaNEP) and the European network FUNCARS for financial support. M.M.F. and F.Z. would like to acknowledge support from the Italian FIRB project “Carbonio micro e nanostrutturato.”

*Electronic address: pascal.ruffieux@empa.ch

[1] M. F. Crommie, C. P. Lutz, and D. M. Eigler, Nature (London) **363**, 524 (1993).

[2] J. Repp, F. Moresco, G. Meyer, K. Rieder, P. Hyldgaard, and M. Persson, Phys. Rev. Lett. **85**, 2981 (2000).

[3] P. T. Sprunger, L. Petersen, E. W. Plummer, E. Lægsgaard, and F. Besenbacher, Science **275**, 1764 (1997).

[4] L. Peterson, B. Schaefer, E. Lægsgaard, I. Stensgaard, and F. Besenbacher, Surf. Sci. **457**, 319 (2000).

[5] J. I. Pascual, G. Bihlmayer, Yu. M. Koroteev, H.-P. Rust, G. Ceballos, M. Hansmann, K. Horn, E. V. Chulkov, S. Blügel, P. M. Echnique, and Ph. Hofmann, Phys. Rev. B **63**, 241103 (2001).

[6] M. Vershinin, S. Misra, S. Ono, Y. Abe, Y. Ando, and A. Yazdani, Science **303**, 1995 (2004).

[7] H. A. Mizes and J. S. Foster, Science **244**, 559 (1989).

[8] P. Ruffieux, O. Gröning, P. Schwaller. L. Schlapbach, and P. Gröning, Phys. Rev. Lett. **84**, 4910 (2000).

[9] Z. Klusek, Appl. Surf. Sci. **125**, 339 (1997).

[10] M. Bockrath, W. Liang, D. Bozovic, J. H. Hafner, C. M. Lieber, M. Tinkham, and H. Park, Science **291**, 283 (2001).

[11] H. J. Choi and J. Ihm, Phys. Rev. Lett. **84**, 2917 (2000).

[12] H. W. Ch. Postma, T. Teepen, Z. Yao, M. Grifoni, and C. Dekker, Science **293**, 76 (2001).

[13] P. Ruffieux, O. Gröning, M. Bielmann, P. Mauron, L. Schlapbach, and P. Gröning, Phys. Rev. B **66**, 245416 (2002).

[14] D. Tománek, S. G. Louie, H. J. Mamin, D. W. Abraham, R. E. Thomson, E. Ganz, and J. Clarke, Phys. Rev. B **35**, 7790 (1987).

[15] F. Atamny, O. Spillecke, and R. Schlögl, Phys. Chem. Chem. Phys. **1**, 4113 (1999)

[16] P. Blaha, K. Schwarz, and J. Luitz, WIEN97, Vienna University of Technology 1997. [Improved and updated Unix version of the original copyrighted WIEN-code, which was published by P. Blaha, K. Schwarz, P. Sorantin, and S. B. Trickey, in Comput. Phys. Commun. **59**, 399 (1990).]

[17] C. L. Kane and E. J. Mele, Phys. Rev. B **59**, R12 759 (1999).

[18] The expected wave vector for small momentum scattering is given by $k = Ue/\hbar v_F$ (v_F is the Fermi velocity; for graphite: $v_F = 8\times10^5$ m/s resulting in a wavelength of the charge modulation of $\sim$50 nm (sample bias $U = 70$ mV). Even if such modulations were present, they could not be resolved from the FFT analysis of the STM images, since the intensity around $k = 0$ is dominated by the local charge enhancement near the defects.

[19] S. G. Lemay, J. W. Janssen, M. van den Hout, M. Mooij, M. J. Bronikowski, P. A. Willis, R. E. Smalley, L. P. Kouwenhoven, and C. Dekker, Nature (London) **412**, 617 (2001).

[20] K. F. Kelly and N. J. Halas, Surf. Sci. **416**, L1085 (1998).

[21] M. S. Dresselhaus, G. Dresselhaus, and R. Saito, Phys. Rev. B **45**, 6234 (1992).